Langmuir

Article

pubs.acs.org/Langmuir

From Hydrodynamic Plumes to Chemical Gardens: The Concentration-Dependent Onset of Tube Formation

Bruno C. Batista, Patrick Cruz, and Oliver Steinbock*

Department of Chemistry and Biochemistry, Florida State University, Tallahassee, Florida 32306-4390, United States

Supporting Information

ABSTRACT: Many inorganic precipitation reactions self-organize macroscopic tubes known as chemical gardens. We study the nonequilibrium formation of these structures by injecting aqueous sodium sulfide solution into a reservoir of iron(II) chloride solution. Our experiments reveal a distinct, concentration-dependent transition from convective plumes of reaction-induced, colloidal particles to mechanically connected, hollow tubes. The transition concentration (0.1 mol/L) is widely independent of the injection rate and causes a discontinuous change from the radius of the plume stalk to the radius of the tube. In addition, tubes have lower growth speeds than plumes. At the transition concentration, one observes the initial formation of a plume followed by the growth of a mechanically weak tube around a jet of upward-moving precipitation particles. We find that the plumes' morphology and geometric scaling are similar to that of laminar starting plumes in nonreactive systems. The characterization of dried tubes by X-ray diffraction indicates the presence of greigite and lepidocrocite.

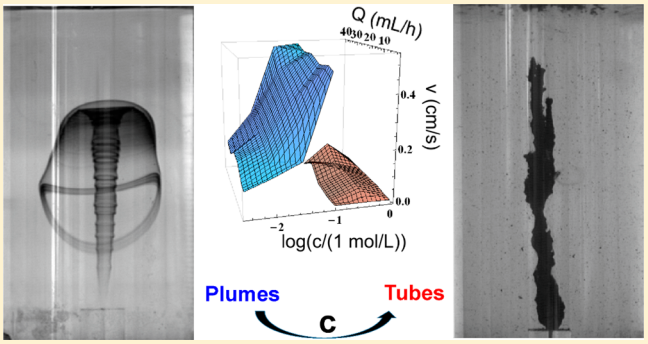

INTRODUCTION

When two solutions containing reactive species come in contact, complex reaction-transport mechanisms unfold in space and time. These nonequilibrium processes can create surprising spatiotemporal patterns and materials that differ from those obtained in conventional mixing experiments.[1,2] Liesegang rings are a classic example of this scenario.[3] They result from the reaction of inorganic ions or charged nanoparticles and consist of bandlike precipitation patterns.[4,5] Recent studies demonstrated that these structures can extend down to length scales of tens of nanometers. They are controllable using wet-stamping techniques and allow the production of structures such as Fresnel lenses.[6−8] All of these advances suggest great potential for the production of microdevices based on reaction−diffusion processes.

Another classic example is a family of tubular precipitation structures which are often referred to as chemical gardens.[9] These tubes are the focus of our investigation. Their thin-walled structures typically form from metal ions and oxoanions such as silicates, carbonates, borates, and phosphates.[10] Cronin et al. also demonstrated the production of microtubes from polyoxometalates and organic cations.[11] Very similar tube structures are found in corrosion systems and in setting cement.[12,13] Moreover, Cartwright et al. discussed striking similarities between chemical gardens and hollow ice tubes (brinicles) that form under floating sea ice.[14]

Depending on the choice of reactants and reaction conditions, the length of precipitation tubes in chemical gardens can easily exceed several centimeters whereas their outer diameter is typically in the micro- to millimeter range.[10] In the case of the classic silica tubes, the wall consists of amorphous silica and metal hydroxides (and/or oxides) that follow opposing compositional gradients in the radial direction.[9,15,16] Recent studies also reported the synthesis of superparamagnetic silica−magnetite tubes, tubes with trapped quantum dots, photocatalytically active structures, and postsynthetic modifications.[17−20]

While many studies in this field initiate tube growth from a small seed particle,[21,22] other approaches involve the steady injection of one reactant solution (e.g., $CuSO_4$(aq)) into a large reservoir of another reactant (e.g., sodium silicate).[23−27] Using the latter technique, four distinct growth regimes were identified: (i) jetting, for which the open tube forms around a buoyant jet of reactant solution, (ii) popping, for which the tube is capped by a thin balloonlike membrane that expands and detaches periodically, (iii) budding, which is similar to (ii) but involves rupturing rather than the detachment of the expanding membrane, and (iv) fracturing, which is also similar to (ii) but involves the detachment of longer and more rigid tube segments.[23,26] During the past decade, several aspects of these different growth modes have been studied quantitatively and some were described successfully by mathematical models. Examples include the tube radius under jetting growth, the detachment period of popping tubes, and pressure oscillations

Received: May 26, 2014
Revised: July 9, 2014
Published: July 11, 2014

   dx.doi.org/10.1021/la5020175 | Langmuir 2014, 30, 9123−9129

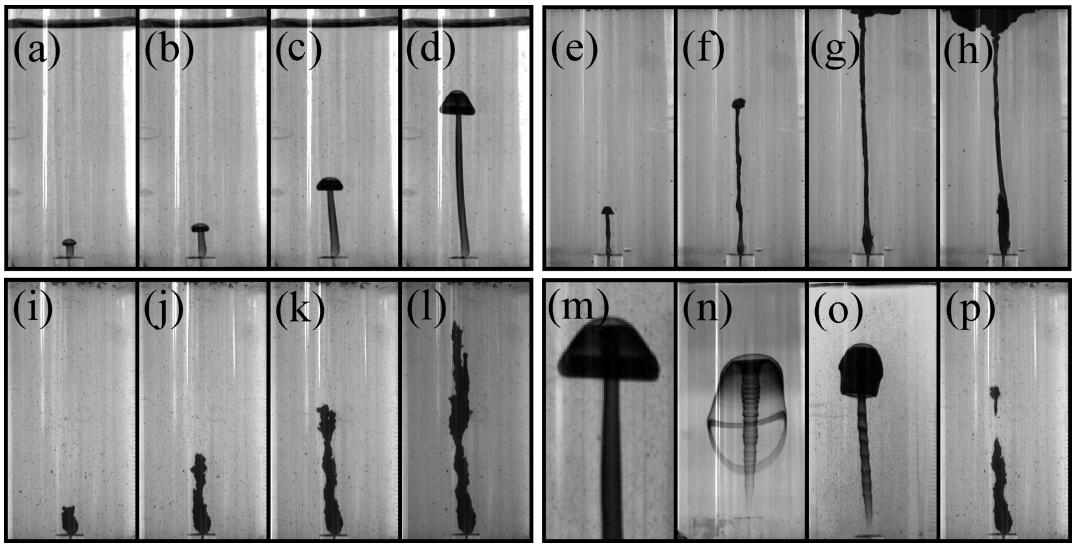

Figure 1. Overview of different growth regimes and structures. (a–d) Image sequence of a plume (c = 0.01 M). (e–h) Image sequence of a plume templating the subsequent growth of a tube (c = 0.1 M). (i–l) Image sequence of a growing tube (c = 0.317 M). The photographs in (m–o) illustrate different plume morphologies and (p) shows an example of noncontinuous tube growth. Pump rate Q in mL/h: 8 (a–d, m, p), 16 (e–h), 8 (i–l), and 32 (n, o). The image sequences starting with (a), (e), and (i) span 40, 120, and 110 s, respectively. Field of view: 6.3 mm × 3.4 mm (a–l, n–p) and 2.5 mm × 1.3 mm (m).

within closed tube structures.[23−28] Nonetheless, many important questions remain unanswered, and the fundamental goal of predicting whether a certain precipitation reaction can produce tubular structures has remained elusive.

There is also increasing interest in the role that similar structures and materials might have played in the emergence of life.[29−32] Russell et al. suggested that prebiotic chemistry started in the walls of chimney structures formed at off-axis alkaline vents on the ocean floor.[33,34] These precipitates possibly offered the needed combination of porosity and catalytic activity as well as geochemically sustained gradients in pH and temperature. The catalytic activity likely resulted from iron–nickel sulfides that formed when the warm hydrothermal fluid surged into the acidic, anoxic, and ferrous ion-containing Hadean ocean.[35] The hydrothermal fluid is seawater altered by underground serpentization and most likely contained hydrogen sulfide ions, hydrogen gas, methane, carbon monoxide, and other species.[34]

In this Article, we employ two of the reactants discussed in the context of the origin-of-life theories proposed by Russell, Wächtershäuser, and others.[33−35] By analogy to off-axis alkaline vents, we inject sodium sulfide solution into a large water reservoir containing ferrous ions. We specifically investigate the parameter-dependent onset of tube formation and determine the concentration threshold below which tube formation does not occur. Our results show that tube growth is closely related to the aggregation of precipitate particles and their mechanical cohesion. Below the threshold, striking hydrodynamic plumes are observed that display scaling laws expected for starting plumes in nonreactive fluids.

EXPERIMENTAL SECTION

All solutions are prepared using nanopure water (18 MΩ cm, Barnstead Easypure UV), $FeCl_2{\cdot}4H_2O$ (J. T. Baker), and Na_2S (Sigma-Aldrich). In the typical experiment, sodium sulfide solution is pumped at a constant rate through a glass capillary (inner diameter 0.6 mm) into a cylindrical glass chamber (diameter 3 cm) containing 50 mL of the ferrous solution. The ratio between the concentrations of iron and sulfide ions is kept constant at 1.0. The two reactant concentrations c and the pump rate Q are varied in the range of 3.17 mmol/L to 1.0 mol/L and 1 mL/h to 40 mL/h, respectively. We investigate the resulting two-dimensional parameter space at 54 different points. For each of these experimental conditions, we record image sequences of the reaction system with a monochrome charge-coupled device camera (COHU 2122) connected to a personal computer via a frame-grabber board (Data Translation DT3155, 640 pixels × 480 pixels at 8 bit/pixel). These images are captured at a rate of 2 frames/s and analyzed using in-house software.

The materials characterization of the solid tubes is carried out according to the following procedure. We synthesize precipitation tubes at equal reactant concentrations of c = 1.0 mol/L and for a flow rate of Q = 8.0 mL/h. After a given tube has reached a vertical length of 5 cm, it is collected with a glass tube and transferred to a beaker containing water. During this procedure, the tubes always break into several segments. After the collection of ten samples, the resulting material is filtered, washed again, and then dried under ambient conditions unless noted otherwise. The resulting solids are then ground and analyzed by powder X-ray diffraction (PANanalytical X'Pert PRO) operating at the Cu Kα emission line (wavelength 1.5418 Å).

RESULTS AND DISCUSSION

Figure 1(a-l) illustrates three distinct growth modes that are observed when sodium sulfide solution is injected into a large reservoir of ferrous chloride solution. At low reactant concentration (a–d), a striking plume structure forms that rises to the top of the reactant container. Notice that the umbrella-like plume head is followed by a smooth cylindrical conduit. Both the head and the conduit consist of small, black particles that form when the two solutions come in contact. While we did not attempt to characterize these reaction-induced colloidal particles, other reports[36] strongly suggest that they consist of mackinawite, which is a form of iron sulfide.

Plume structures are observed up to a concentration of 0.1 mol/L, beyond which they give way to the formation of hollow tubes. At the transition concentration, we observe the growth behavior shown in Figure 1(e–h). Initially, a thin dark conduit forms, featuring an enlarged top end that is reminiscent of the umbrella-shaped plume head observed at lower concentrations.

dx.doi.org/10.1021/la5020175 | Langmuir 2014, 30, 9123–9129

This structure can be easily disrupted by stirring. Once it reaches the top of the reaction vessel, it starts to accumulate buoyant material (g). Subsequently a thickening of its base occurs that slowly grows in the upward direction. The latter step creates a mechanically connected hollow tube. This structure is very fragile and does not allow the collection of fragments for further characterization.

At higher concentrations, this jet-templated tube growth is replaced by the dynamics shown in image sequence (i–l). In this third growth regime, the tubes start to form immediately when the sulfide solution is injected, and they do not show any noticeable thickening in the outside direction. The structures show erratic deviations from a smooth cylindrical shape, which clearly distinguishes them from the plume conduits at lower concentrations. In addition, they are sturdier than the tubes formed at the transition point. At concentrations greater than or equal to 0.1 mol/L, we always observe the formation of single tubes although some local branching is observed at high flow rates.

Figure 1(m–o) show three examples of different plume morphologies observed in our experiments. Image (m) is a magnification of the structure shown in (d). The head is compact and tightly confined to a cone. The plume structures in Figure 1(n,o) are found at high flow rates and feature a longer skirtlike head. Notice the spatially periodic pattern along the conduit in (o) (and (n)). It is not clear whether this pattern is caused by hydrodynamics or a weak interaction between the colloidal particles. However, elastic deformations of a membranelike skin can be ruled out. We note that this crinkling of the plume conduit is observed only at high pump rates.

A visual inspection of the video data shows that the tightly confined heads involve a ring-shaped vortex while such convection structures seem to be absent in the skirtlike heads. Lastly, Figure 1(p) illustrates a variant of the simple tube growth shown in (i–l). Here several millimeter-long tube segments detach from the main structure and rise toward the top of the reaction vessel. This behavior is found around a reactant concentration of 0.3 mol/L and typically affects early tube structures with lengths below 3 to 4 cm. We note that the latter dynamics is very similar to the fracturing behavior discussed by Pagano et al. for tube growth caused by the injection of sodium silicate solution into a large volume of copper sulfate solution.[26]

The differences between tube growth and plume dynamics also manifest themselves in quantitative aspects. Figure 2a shows the growth velocity of these structures for 54 different pump rates (Q) and reactant concentrations (c). Notice that the latter quantity is plotted on a logarithmic scale. The growth rate is measured as the vertical speed of the plume head or the top of the tube. Whereas the velocity of the tubes shows no measurable dependence on the height, the plume heads initially accelerate during their ascent.[37] We therefore measure the average plume speed from the upper half of the vessel where the velocity is nearly constant. In addition, we use different colors to distinguish between data from plumes (blue, labeled p) and tubes (red, labeled t). This assignment is made based on the visual differences shown in Figure 1.

Our measurements of the growth rates reveal two distinct surfaces. Below the transition concentration, plume growth is characterized by high growth speeds that increase with increasing concentration. Tube growth, however, is much slower and shows no clear dependence on the reactant

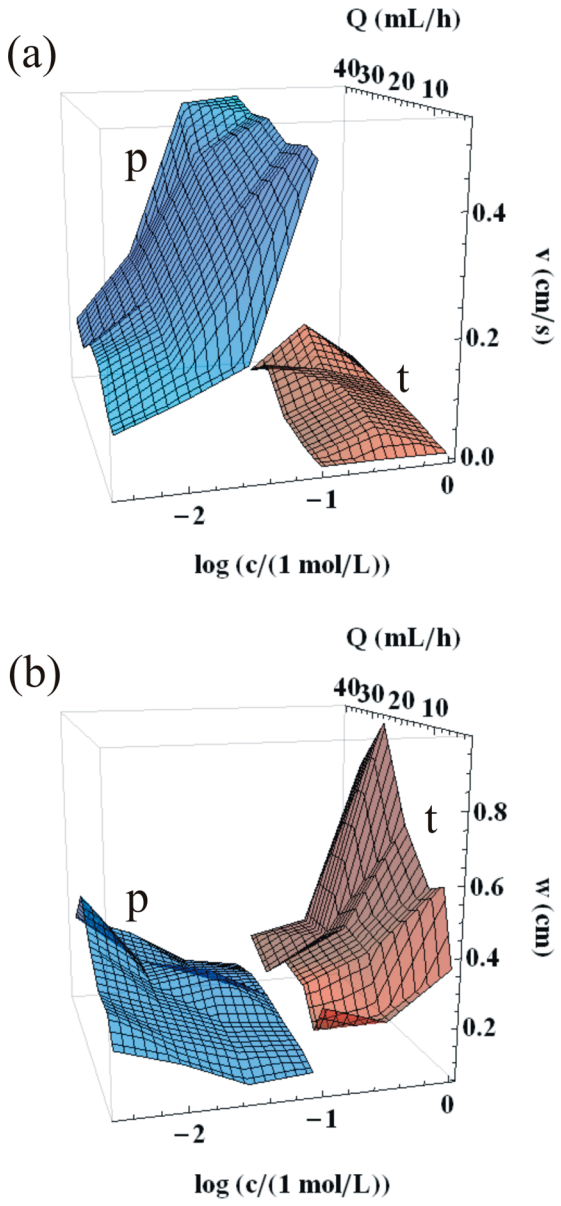

Figure 2. (a) Velocity of the rising plumes (p, blue) and upward-growing tubes (t, red) as a function of the pump rate Q and the reactant concentration c. (b) Average width of the plume conduits (p, blue) and the tube structures (t, red) as a function of Q and c.

concentration. Moreover, we find that the transition concentration does not change over the range of the investigated pump rates (1–40 mL/h). At the transition, we observe, as stated before, the initial ascent of a plumelike structure followed by tube growth around the plume conduit (Figure 1(e–h)). Accordingly, we plot both speeds, which results in an overlap of the plume and tube surfaces.

Figure 2b characterizes the width of the observed structures for the same range of pump rates and reactant concentrations. These widths describe the average, outer diameter of the hollow tubes and the diameter of the plume conduits. The width of the umbrella-shaped plume head is not considered for this specific analysis. The figure is organized in the same way as Figure 2a and uses blue and red shades for plume and tube data, respectively. We find that for plumes, the width decreases with increasing concentration of the reactants; the tube data, however, show the opposite dependence. Moreover, the

dx.doi.org/10.1021/la5020175 | Langmuir 2014, 30, 9123–9129

width increases with increasing pump rates for both the plume conduits and the precipitation tubes. Notice the discontinuity at the transition concentration, which corresponds to the unusual growth around a very thin reactant jet. The jump in width is approximately 1.5 mm, which suggests 0.75 mm as a good estimate for the thickness of the forming cylindrical envelope. We reemphasize that these structures are mechanically weak and cannot be extracted. Even at the highest reactant concentration investigated (1.0 mol/L), we could extract only tube fragments for further characterization.

The value of 0.75 mm can be compared to the wall thickness measured from injection experiments that use other tube-forming precipitation reactions but similar pump rates and concentrations. Pagano and Steinbock, for instance, studied a silica/copper(II) system and found that the dried tubes had a wall thickness of about 10 μm, which appears to be typical for macroscopic tubes formed by injection experiments.[15] However, even if we assume that the wall shrinks by a factor of 10 during drying, the resulting value is about 7 times smaller than the thickness of the thick cylindrical envelopes at the transition concentration (Figure 1(h)). This finding shows that these structures are qualitatively different from solid tubes and hence suggests an interpretation of the wall as dense particle aggregates. At higher ionic strengths and higher concentrations of iron and sulfide ions, we successfully extracted tube fragments and found wall thicknesses around the expected value of 10–20 μm (Figure S1).

Figure 3 combines the data from Figure 2 into a single plot of growth rates and widths. It encompasses the entire range of

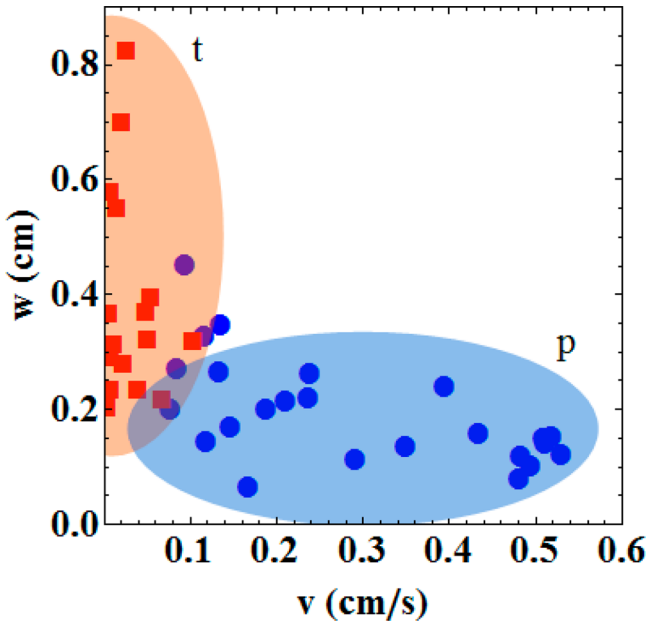

Figure 3. Velocity v and width w of the rising plumes (blue circles) and upward-growing tubes (red squares) as measured over a wide range of reactant concentrations and pump rates. The blue and red areas are meant as a guide to the eye and encompass most of the plume and tube data, respectively.

pump rates and reactant concentrations studied here. We find that tube formation is characterized by growth rates below approximately 0.1 cm/s and can give rise to a wide range of outer diameters. The plume conduits, however, are mainly constrained to diameters below 0.2 cm and have a wide range of velocities. We highlight this grouping qualitatively by the two elliptical areas in Figure 3. The overlap between these areas does not correspond to results obtained at the transition concentration because the latter involve fast plume growth (Figure 2(a)).

The special nature of the system dynamics at the transition concentration extends to other characteristics such as the structures' average rate of volume increase. For a closed structure the increase in volume should essentially match the volume of the injected solution, whereas an open structure shows a much lower rate of volume increase. Examples for these two distinct dynamic regimes were first clearly described in ref 23 for the example of silica–copper–hydroxide tubes and are usually associated with jetting and popping/budding growth, respectively.

Figure 4 shows the rate of the increasing tube volume as a function of the employed pump rate for our iron sulfide system.

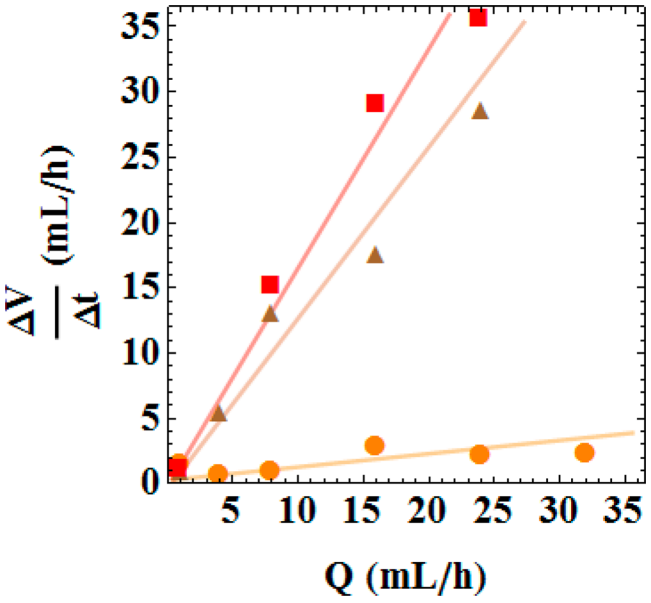

Figure 4. Rate of increase in the volume of tubes as a function of the pump rate. The reactant concentrations are 0.1 (circles), 0.317 (triangles), and 1.0 mol/L (squares). The continuous lines are obtained by linear regression analysis of the three corresponding data sets.

Circular, triangular, and square markers correspond to reactant concentrations of 0.1 (the transition point), 0.317, and 1.0 mol/L, respectively. The tube volume ΔV is measured from video images as $\pi A^2/(4h)$ where A and h denote the image area enclosed by the tube's outer contour and its height, respectively. This method tends to overestimate the volume due to deviations of the tubes from a perfect cylindrical shape.

The results in Figure 4 show that tubes formed at high concentrations conserve the volume of the injected solution. The actual proportionality factors are 1.7 and 1.3 for 1.0 and 0.317 mol/L, respectively. These factors are both larger than the expected value of 1.0 for closed tubes. We attribute this deviation to the aforementioned limitation of the employed method. Notice that it is not reasonable to interpret these values as reaction-induced volume contributions because the solid phase is minute compared to the enclosed liquid. The results for 0.1 mol/L yield a proportionality factor of 0.11 which reemphasizes that these tubelike structures are open and

dx.doi.org/10.1021/la5020175 | Langmuir 2014, 30, 9123–9129

grow around a buoyant jet of reactant solution. Since this jet must induce convection in the surrounding iron solution, we interpret this finding as additional evidence for mechanical cohesion within the aggregate-like wall.

All of these observations suggest strongly that the tube growth at the transition concentration is very similar to the jet-templated growth described by Stone et al. for the reaction of aqueous NH_3 and NH_4^+ species injected into a large reservoir containing iron(II) sulfate solution.[38] In addition, we emphasize that the closed tube structures at higher concentrations are a qualitatively new growth regime that differs from the ones described by Thouvenel-Romans and Steinbock.[23] In the latter study, closed growth was always associated with oscillatory (or at least rhythmic) events in which either balloonlike tube segments detached from the tube's top or new tube segments formed in a budding process.

As mentioned earlier, tubes formed at higher concentration can be extracted from the reactor but break into small, macroscopic fragments during transfer. These fragments, as obtained from about 10 individual tubes (total length of approximately 40 cm), are washed in water to remove unreacted solution and then dried under ambient conditions. To obtain insights into the chemical composition of the tube wall, we perform X-ray diffraction (XRD) measurements on the resulting powder samples. The diffraction pattern is shown in Figure 5 and cannot be explained in terms of a single species.

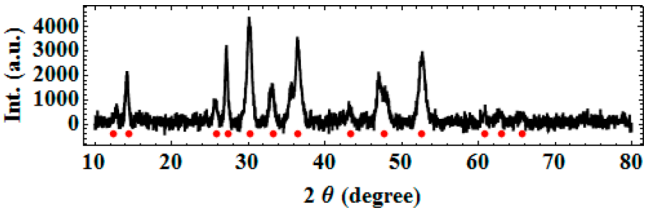

Figure 5. X-ray diffraction pattern of precipitation tubes dried under ambient conditions. The red circles indicate peak positions. The samples were produced for reactant concentrations of 1.0 mol/L and a pump rate of 8.0 mL/h.

The main constituents are Fe_3S_4 (greigite) and FeOOH (lepidocrocite).[31] In addition, there is evidence for the presence of $FeS{\cdot}H_2O$ (melkovite) and elemental sulfur.

The chemistry of iron sulfides is particularly rich.[39] For conventional mixing experiments with aqueous ferrous and sulfide ions and for concentrations comparable to the ones explored here, mackinawite (FeS) nanoparticles are known to be the dominant product.[36] When this material is exposed to molecular oxygen, it easily converts to the mixed-valence compound greigite and elemental sulfur.[40] Furthermore, greigite is not stable and reacts to form iron oxides and iron oxyhydroxides.[41] This reaction sequence is in good agreement with our assignments of the XRD pattern.

Since molecular oxygen plays a significant role in defining the chemical nature of the tubes, we prepared additional samples under an inert gas (N_2) atmosphere. Once the dried material is exposed to air, one notices spontaneous heat production caused by hydration and/or oxidation reactions. Moreover, we observed an interesting color change for tubes produced under aerobic conditions that can be interpreted in the same context. If the tube is left in the reaction solution for several hours, then it changes color from black to orange. This process is accelerated by increasing the concentration of dissolved oxygen in the solution. All of these findings suggest that oxidation processes produce lepidocrocite FeOOH, which is known to be an orange compound, thus further supporting our XRD assignment.

Lastly, we analyze the structure of the hydrodynamic plumes observed at low reactant concentrations. Such structures form when a fluid discharges from a single submerged orifice. Most authors distinguish between the limiting cases of jets, which are driven by their initial momentum, and plumes, which are driven by buoyancy.[42] The relative strength of these two factors is expressed by the Richardson number, *Ri*, which is defined as

$$Ri = g(\rho_o - \rho_i)d/(\rho_o v_h^2)$$

where g, d, and v_h denote the acceleration due to earth's gravity, the diameter of the orifice, and the ascent velocity of the plume head, respectively. The densities ρ_o and ρ_i correspond to the outer, ambient fluid and the injected solution, respectively. The second dimensionless number often used for the description of plumes is the Reynolds number, *Re*, given by

$$Re = 4Q/\pi\nu_i d$$

where ν_i is the kinematic viscosity of the injected solution. Here we are using the standard Reynolds number for the flow in the injection tube,[42] which is based on the capillary's inner diameter and averaged flow velocity. The concentration-dependent densities and the kinematic viscosity are specified in the Supporting Information.

Figure 6(a) shows a double-logarithmic plot of *Ri* versus *Re* for the plumes observed in our experiments. The range of measured *Ri* values (0.3−3) shows that our plumes are affected by both buoyancy and initial momentum, whereas the small values of the Reynolds numbers indicate laminar flow rather than turbulence. In addition, we find that the experimental data are described by a power law of the form $Ri \propto Re^k$. Linear fitting yields a power law exponent of $k = -0.62 \pm 0.09$ for the entire set of data shown (straight line in Figure 6(a)). This finding is qualitatively similar to results by Rogers and Morris for nonreactive plumes.[42] Their experiments employed simple glycerol−water solutions and visualized the plumes by a shadowgraph technique or added dyes. Notice that the power law exponent in their study is $k = -0.96$. Despite this small difference, our measurements show that the plumes in our system are dominated by fluid dynamics rather than chemical processes.[43,44]

Rogers and Morris also distinguished between tightly confined and dispersed plume heads.[42] The latter plumes feature a skirtlike structure similar to those shown in our Figure 1(m,n) whereas the confined plume heads are similar to the pattern in our Figure 1(o). The dynamics of the head are reflected in the relative growth rates of its width w_h and length l_h. The associated Reynolds numbers are

$$Re_{hw} = w_h v_h/\nu_i \text{ and } Re_{hl} = l_h v_h/\nu_i$$

Figure 6b shows the scaling behavior of Re_{hw} as a function of Re_{hl} obtained from experiments at six different pump rates between 4 and 40 mL/h. Each data set follows an initially linear dependence but later decreases in slope to saturate at a nearly constant Re_{hw}. The linear portions of the six data sets fall on one master curve described by $Re_{hw} = 1.4Re_{hl}$. Also note that the width is always larger than the height of the plumes. Again these findings are at least qualitatively similar to the results reported by Rogers and Morris[42] for nonreactive plumes.

dx.doi.org/10.1021/la5020175 | *Langmuir* 2014, 30, 9123−9129

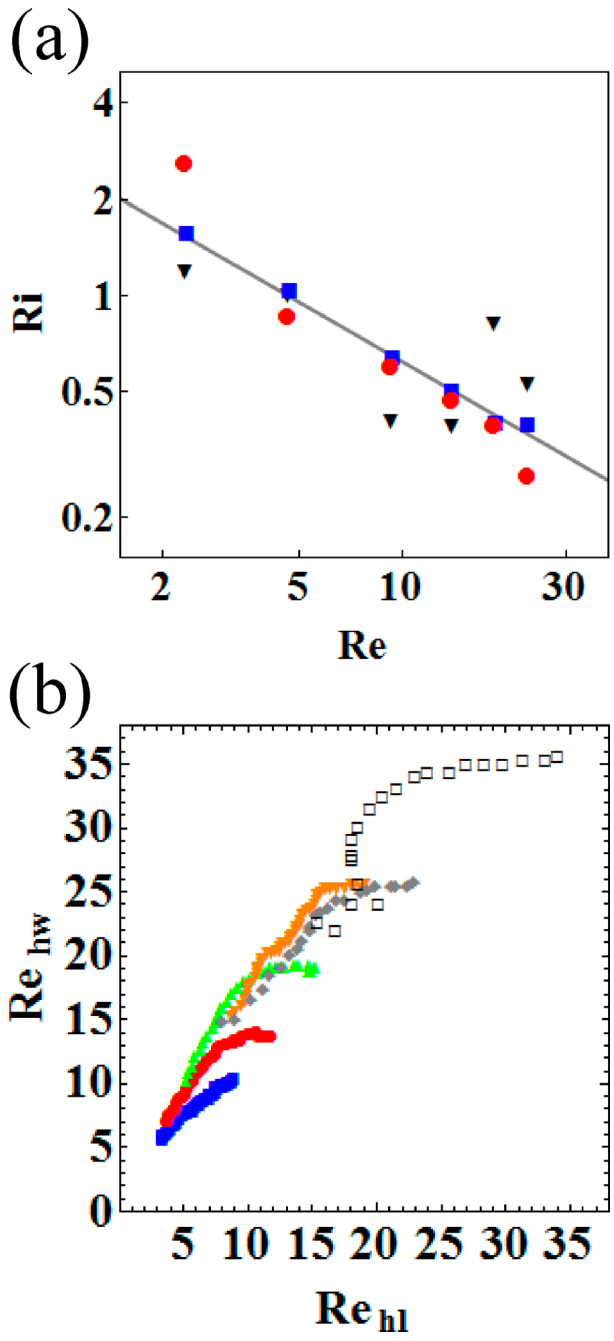

Figure 6. (a) Dependence of the plumes' Richardson number on the Reynolds number of the injected sodium sulfide solution. The three data sets correspond to reactant concentrations of 3.17 mmol/L (black triangles), 0.01 mmol/L (blue squares), and 0.0317 mol/L (red circles). The continuous line is obtained by linear regression analysis of the entire data set. (b) Reynolds number Re_{hw} associated with the width of the plume heads as a function of the Reynolds number Re_{hl} associated with their vertical length. The six data sets correspond to pump rates of 4 (blue squares), 8 (red circles), 16 (green triangles), 24 (orange triangles), 32 (gray diamonds), and 40 mL/h (open squares). The reactant concentrations equal 0.01 mol/L.

CONCLUSIONS

This study establishes that tube growth occurs only above a critical concentration threshold that is widely independent of the employed flow rate. It is reasonable to conclude that this result qualitatively applies to all tube-forming reactions. The specific threshold concentration (0.1 mol/L) is orders of magnitude higher than the solubility of iron sulfide. This result shows that active precipitation reactions are necessary but not sufficient for tube formation. As shown by our results (e.g., Figure 1), it is rather the aggregation of the precipitate particles in the moving solution that determines whether a mechanically connected tube can form. In this context, future studies must aim to characterize the concentration-dependent ζ-potential of the particles. In addition, it should be insightful to evaluate injection nozzles made of different materials to better understand the role of adhesion at the tube's base.

At higher concentrations, we observed a transition from open to closed tube growth. The latter dynamics differ from earlier reported, closed growth modes by the absence of periodic events such as popping or budding. Perhaps more importantly, our results strongly suggest that these hydrated structures contain mackinawite that reacts to greigite and lepidocrocite if exposed to molecular oxygen. Future studies on the role of such precipitates as active host materials for prebiotic processes must hence clearly exclude oxygen. Such materials could then be employed to investigate simple building blocks of prebiotic chemistry such as the formation of peptide bonds. Lastly, we note that our study also contributes to the knowledge base of hydrodynamic plumes. At low concentrations, these structures reveal themselves through particles formed at the reactive interface, which differs qualitatively from the use of dyes or measurements of the refractive index. This feature not only could be a technical advantage for specific measurements but also could give rise to interesting deviations from plumes in nonreactive systems.

ASSOCIATED CONTENT

Supporting Information

Scanning electron micrograph of a tube fragment. Table of physical constants relevant to the analysis of the plume structures. Three movies showing a plume at low concentration (0.01 mol/L), jet-templated tube growth at the transition point (0.1 mol/L), and tube formation at a high concentration (1.0 mol/L). This material is available free of charge via the Internet at http://pubs.acs.org.

AUTHOR INFORMATION

Corresponding Author

*E-mail: steinbck@chem.fsu.edu.

Notes

The authors declare no competing financial interest.

ACKNOWLEDGMENTS

This work is supported by the National Science Foundation under grant no. 1005861. B.C.B. thanks the National Council for Scientific and Technological Development (CNPq, Brazil) for a postdoctoral fellowship.

REFERENCES

(1) Epstein, I. R.; Pojman, J. A. *An Introduction to Nonlinear Chemical Dynamics*; Oxford University Press: New York, 1998.
(2) Grzybowski, B. A. *Chemistry in Motion*; John Wiley and Sons: Chichester, 2009.
(3) Müller, S. C.; Kai, S.; Ross, J. Curiosities in periodic precipitation patterns. *Science* **1982**, *216*, 114−128.
(4) Lagzi, I. Controlling and engineering precipitation patterns. *Langmuir* **2012**, *28*, 3350−3354.

(5) Lagzi, I.; Kowalczyk, B.; Grzybowski, B. A. Liesegang rings engineered from charged nanoparticles. *J. Am. Chem. Soc.* **2010**, *132*, 58−60.
(6) Smoukov, S.K.; Bitner, A.; Campbell, C. J.; Kandere-Grzybowska, K.; Grzybowski, B. A. Nano- and microscopic surface wrinkles of linearly increasing heights prepared by periodic precipitation. *J. Am. Chem. Soc.* **2005**, *127*, 17803−17807.
(7) Grzybowski, B. A.; Bishop, K. J. M.; Campbell, C. J.; Fialkowski, M.; Smoukov, S. K. Micro- and nanotechnology via reaction-diffusion. *Soft Matter* **2005**, *1*, 114−128.
(8) Smoukov, S.K.; Lagzi, I.; Grzybowski, B. A. Independence of primary and secondary structures in periodic precipitation patterns. *J. Phys. Chem. Lett.* **2011**, *2*, 345−349.
(9) Cartwright, J. H. E.; Escribano, B.; Sainz-Díaz, C. I. Chemical-garden formation, morphology, and composition. I. Effect of the nature of the cations. *Langmuir* **2011**, *27*, 3286−3293.
(10) Makki, R.; Roszol, L.; Pagano, J. J. Steinbock, O. Tubular precipitation structures: materials synthesis under non-equilibrium conditions. *Philos. Trans. R. Soc. A* **2012**, *370*, 2848−2865.
(11) Cooper, G. J. T.; Boulay, A. G.; Kitson, P. J.; Ritchie, C.; Richmond, C. J.; Thiel, J.; Gabb, D.; Eadie, R.; Long, D.; Cronin, L. Osmotically driven crystal morphogenesis: a general approach to the fabrication of micrometer-scale tubular architectures based on polyoxometalates. *J. Am. Chem. Soc.* **2011**, *133*, 5947−5954.
(12) Stone, D. A.; Goldstein, R. E. Tubular precipitation and redox gradients on a bubbling template. *Proc. Natl. Acad. Sci. U.S.A.* **2004**, *101*, 11537−11541.
(13) Double, D. D.; Hellawell, A.; Perry, S. J. The hydration of Portland cement. *Proc. R. Soc. London A* **1978**, *359*, 435−451.
(14) Cartwright, J. H. E.; Escribano, B.; González, D. L.; Sainz-Díaz, C. I.; Tuval, I. Brinicles as a case of inverse chemical gardens. *Langmuir* **2013**, *29*, 7655−7660.
(15) Pagano, J. J.; Thouvenel-Romans, S.; Steinbock, O. Compositional analysis of copper-silica precipitation tubes. *Phys. Chem. Chem. Phys.* **2007**, *9*, 110−116.
(16) Roszol, L.; Steinbock, O. Controlling the wall thickness and composition of hollow precipitation tubes. *Phys. Chem. Chem. Phys.* **2011**, *13*, 20100−20103.
(17) Makki, R.; Steinbock, O. Nonequilibrium synthesis of silica-supported magnetite tubes and mechanical control of their magnetic properties. *J. Am. Chem. Soc.* **2012**, *134*, 15519−15527.
(18) Makki, R.; Ji, X.; Matoussi, H.; Steinbock, O. Self-organized tubular structures as platforms for quantum dots. *J. Am. Chem. Soc.* **2014**, *136*, 6463−6469.
(19) Pagano, J. J.; Bánsági, T.; Steinbock, O. Bubble-templated and flow-controlled synthesis of macroscopic silica tubes supporting zinc oxide nanostructures. *Angew. Chem., Int. Ed.* **2008**, *47*, 9900−9903.
(20) Roszol, L.; Makki, R.; Steinbock, O. Postsynthetic processing of copper hydroxide-silica tubes. *Chem. Commun.* **2013**, *49*, 5736−5738.
(21) Maselko, J.; Strizhak, P. Spontaneous formation of cellular chemical system that sustains itself far from thermodynamic equilibrium. *J. Phys. Chem. B* **2004**, *108*, 4937−4939.
(22) Glaab, F.; Kellermeier, M.; Kunz, W.; Morallon, E.; García-Ruiz, J. M. Formation and evolution of chemical gradients and potential differences across self-assembling inorganic membranes. *Angew. Chem., Int. Ed.* **2012**, *51*, 4317−4321.
(23) Thouvenel-Romans, S.; Steinbock, O. Oscillatory growth of silica tubes in chemical gardens. *J. Am. Chem. Soc.* **2003**, *125*, 4338.
(24) Thouvenel-Romans, S.; Steinbock, O. Silica tubes in chemical gardens: radius selection and its hydrodynamic origin. *Europhys. Lett.* **2004**, *67*, 42−48.
(25) Thouvenel-Romans, S.; Pagano, J. J.; Steinbock, O. Bubble guidance of tubular growth in reaction-precipitation systems. *Phys. Chem. Chem. Phys.* **2005**, *7*, 2610−2615.
(26) Pagano, J. J.; Bánsági, T.; Steinbock, O. Tube formation in reverse silica gardens. *J. Phys. Chem. C* **2007**, *111*, 9324−9329.
(27) Tóth, Á.; Horváth, D.; Smith, R.; McMahan, J. R.; Maselko, J. Phase diagram of precipitation morphologies in the Cu^{2+} - PO_4^{3-} system. *J. Phys. Chem. C* **2007**, *111*, 14762−14767.
(28) Pantaleone, J.; Tóth, Á; Horváth, D.; RoseFigura, L.; Morgan, W.; Maselko, J. Pressure oscillations in a chemical garden. *Phys. Rev. E* **2009**, *79*, 056221.
(29) Ruiz-Mirazo, K.; Briones, C.; Escosura, A. Prebiotic systems chemistry: New perspectives for the origins of life. *Chem. Rev.* **2014**, *114*, 285−366.
(30) Mielke, R. E.; Russell, M. J.; Wilson, P. R.; McGlynn, S. E.; Coleman, M.; Kidd, R.; Kanik, I. Design, fabrication, and test of a hydrothermal reactor for origin-of-life experiments. *Astrobiology* **2010**, *10*, 799−810.
(31) Mielke, R. E.; Robinson, K. J.; White, L. M.; McGlynn, S. E.; McEachern, K.; Bhartia, R.; Kanik, I.; Russell, M. J. Iron-sulfide-bearing chimneys as potential catalytic energy traps at life's emergence. *Astrobiology* **2011**, *11*, 933−950.
(32) Barge, L. M.; Doloboff, I. J.; White, L. M.; Stucky, G. D.; Russell, M. J.; Kanik, I. Characterization of iron-phospate-silicate chemical garden structures. *Langmuir* **2012**, *28*, 3714−3721.
(33) Martin, W.; Baross, J.; Kelley, D.; Russell, M. J. Hydrothermal vents and the origin of life. *Nat. Rev.* **2008**, *6*, 805−814.
(34) Russell, M. J.; Nitschke, W.; Branscomb, E. The inevitable journey to being. *Philos. Trans. R. Soc. B* **2013**, *368*, 1−19.
(35) Huber, C.; Wächtershäuser, G. Peptides by activation of amino acids with CO on (Ni,Fe)S surfaces: implications for the origin of life. *Science* **1998**, *281*, 670−672.
(36) Rickard, D.; Griffith, A.; Oldroyd, A.; Butler, I. B.; Lopez-Capel, E.; Manning, D. A. C.; Apperley, D. C. The composition of nanoparticulate mackinawite, tetragonal iron(II) monosulfide. *Chem. Geol.* **2006**, *235*, 286−298.
(37) Kaminski, E.; Jaupart, C. Laminar starting plumes in high-Prandtl-number fluids. *J. Fluid Mech.* **2003**, *478*, 287−298.
(38) Stone, D. A.; Lewellyn, B.; Baygents, J. C.; Goldstein, R. E. Precipitative growth templated by a fluid jet. *Langmuir* **2005**, *21*, 10916−10919.
(39) Rickard, D.; Luther, G. W., III Chemistry of iron sulfides. *Chem. Rev.* **2007**, *107*, 514−562.
(40) Boursiquot, S.; Mullet, M.; Abdelmoula, M.; Génin, J.-M.; Ehrhardt, J.-J. The dry oxidation of tetragonal FeS_{1-x} mackinawite. *Phys. Chem. Miner.* **2001**, *28*, 600−611.
(41) Bourdoiseau, J.-A.; Jeannin, M.; Sabot, R.; Rémazeilles, C.; Refait, Ph. Characterisation of mackinawite by Raman spectroscopy: Effects of crystallization, drying and oxidation. *Corros. Sci.* **2008**, *50*, 3247−3255.
(42) Rogers, M. C.; Morris, S. Natural versus forced convection in laminar starting plumes. *Phys. Fluids* **2009**, *21*, 083601.
(43) Rogers, M. C.; Mantle, M. D.; Sederman, A.J.; Morris, S. Conduits of steady-state autocatalytic plumes. *Phys. Rev. E* **2008**, *77*, 026105.
(44) Rogers, M. C.; Morris, S. The heads and tails of buoyant autocatalytic balls. *Chaos* **2012**, *22*, 037110.